Supplementary Materials

Defining subpopulations of differential drug response to reveal novel target populations

Nirmal Keshava [1,#], Tzen S. Toh [2,3,#], Haobin Yuan [4], Bingxun Yang [4], Michael P. Menden [5,6,7,*], Dennis Wang [3,4,8,*]

1. Constellation Analytics, LLC., Needham MA, USA
2. The Medical School, University of Sheffield, Sheffield, S10 2RX, UK
3. Sheffield Institute for Translational Neuroscience, University of Sheffield, Sheffield, S10 2HQ, UK
4. Department of Computer Science, University of Sheffield, Sheffield, S1 4DP, UK
5. Institute of Computational Biology, Helmholtz Zentrum München - German Research Center for Environmental Health, 85764 Neuherberg, Germany
6. Department of Biology, Ludwig-Maximilians University Munich, 82152 Martinsried, Germany
7. German Centre for Diabetes Research (DZD e.V.), 85764 Neuherberg, Germany
8. NIHR Sheffield Biomedical Research Centre, Sheffield, S10 2HQ, UK

[#] These authors contributed equally to this work.
* These authors are corresponding authors.
Contacts: Michael P. Menden (michael.menden@helmholtz-muenchen.de) or Dennis Wang (dennis.wang@sheffield.ac.uk)

Contents

Comparison of SEABED Segmentation Results with Existing Methods

To yield meaningful and usable subpopulations, we considered the performance of SEABED with respect to hierarchical clustering (Euclidean Minimum Distance and single-linkage) and K-Means clustering (Euclidean Minimum Distance). To enable equitable comparisons, both methods were constrained to find the identical number of subpopulations as SEABED. We were primarily concerned with factors impacting segmentation such as selecting the overall dimensionality of the decomposition, the aggregate separability of the subpopulations, and the size of the subpopulations. The latter two factors are especially important since they directly impact the ability to reliably extract distinct biomarkers.

Two compounds, PLX4720-2 (BRAF inhibitor) and PI-103 (PI3K inhibitor), were examined in Fig. 3 using SEABED. Using the same number of subpopulations found by SEABED, 25, we also executed hierarchical clustering and K-Means to also be evaluated for 25 subpopulations. Our results in Supplementary Table S2 demonstrate that SEABED identifies the most balanced subpopulation sizes, with the largest minimum and median subpopulation size, which is conducive to finding biomarkers. Similarly, we evaluated two different cluster validation measures to evaluate the uniqueness of each pair of subpopulations. Our results in Supplementary Table S3 demonstrate that SEABED finds competitive separation values for the silhouette metric and also has the highest subpopulation homogeneity (RMSSTD). Furthermore, SEABED did not require a prior definition of the number of subpopulations, which is a mandatory input for K-Means.

Finally, we investigated what biomarkers were found by K-Means and hierarchical clustering for the drug pair in Fig. 3b (PLX4720-2 (BRAF inhibitor) and PI-103 (PI3K inhibitor)). In Supplementary Fig. S6, the results for SEABED are compared to the two competing methods. Hierarchical clustering produced one large cluster and several singleton results, making biomarker discovery in sensitive regions impractical. K-Means clustering found two subpopulations enriched for *BRAF* mutations, but with higher P-values. For K-Means clustering, the divergent region had more subpopulations, but they were substantially smaller than the ones found by SEABED.

Supplementary Figures

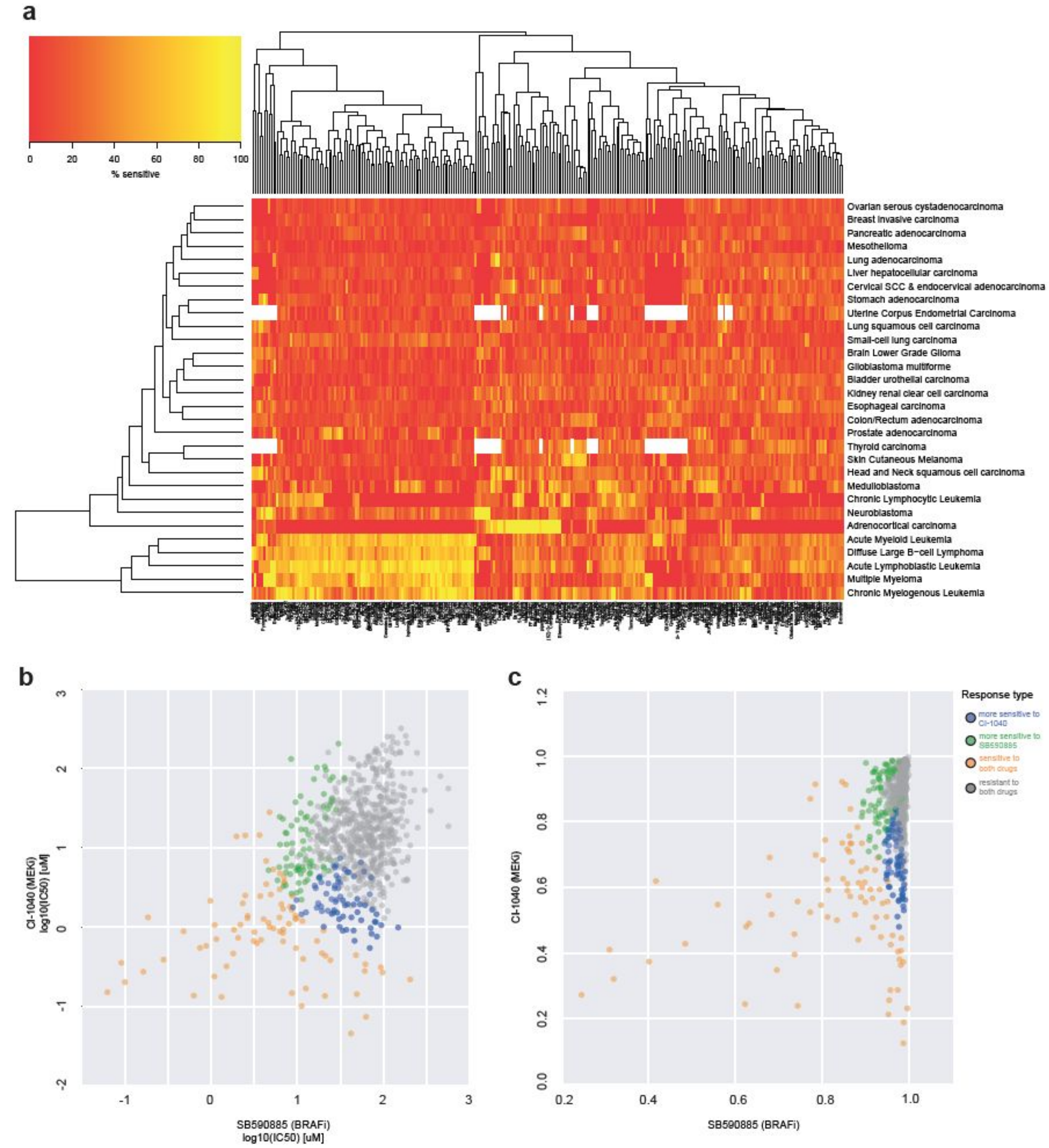

Supplementary Fig. S1 Differences in evaluating drug response individually and by comparing two drugs through segmentation. (A) Heatmap showing the global monotherapy response within 30 different cancer types (vertical axis) treated with 265 drugs (horizontal axis). The range of colours illustrates the percentage of cell lines of a particular cancer type that are sensitive to a given drug, with red being a lower percentage and yellow being a higher percentage. **(B)** Scatter plot showing the log(IC_{50}) values of individual cell lines coloured by the subpopulation they belong to (**Fig. 1c**). Segmentation was carried out based on their response to a BRAF inhibitor (SB590885) and a MEK inhibitor (CI-1040). **(C)** Similar to **(B)** but showing the AUC values of individual cell lines.

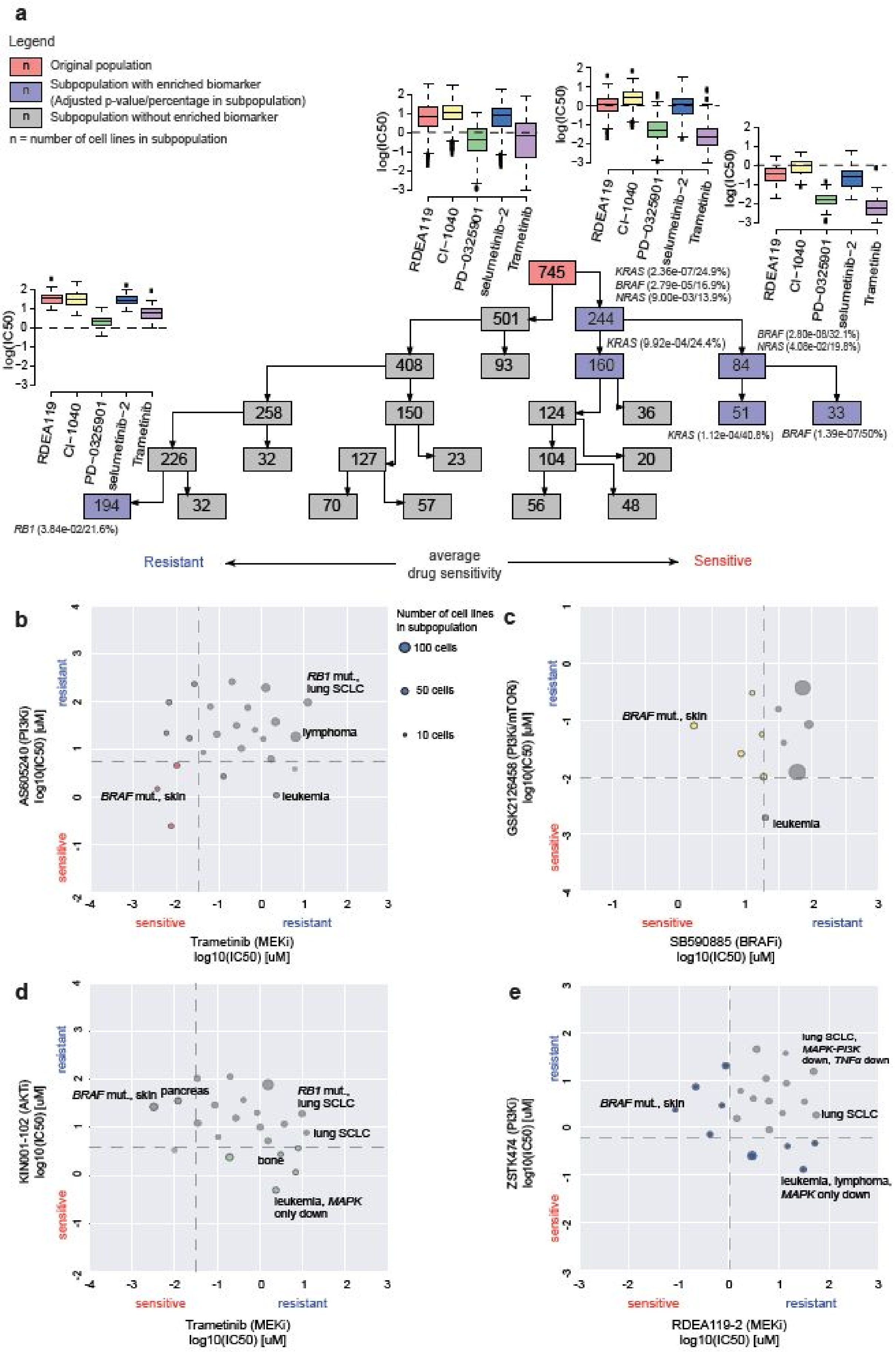
a
Legend
n Original population
n Subpopulation with enriched biomarker (Adjusted p-value/percentage in subpopulation)
n Subpopulation without enriched biomarker
n = number of cell lines in subpopulation
log(IC50)
RDEA119
CI−1040
PD−0325901
selumetinib−2
Trametinib
745
501
244
408
93
160
84
258
150
124
36
51
33
226
32
127
23
104
20
194
32
70
57
56
48
KRAS (2.36e-07/24.9%)
BRAF (2.79e-05/16.9%)
NRAS (9.00e-03/13.9%)
KRAS (9.92e-04/24.4%)
BRAF (2.80e-08/32.1%)
NRAS (4.06e-02/19.8%)
KRAS (1.12e-04/40.8%)
BRAF (1.39e-07/50%)
RB1 (3.84e-02/21.6%)
Resistant
average drug sensitivity
Sensitive
b
AS605240 (PI3K) log10(IC50) [uM]
resistant
sensitive
Number of cell lines in subpopulation
100 cells
50 cells
10 cells
RB1 mut., lung SCLC
lymphoma
BRAF mut., skin
leukemia
Trametinib (MEKi) log10(IC50) [uM]
c
GSK2126458 (PI3K/mTOR) log10(IC50) [uM]
BRAF mut., skin
leukemia
SB590885 (BRAFi) log10(IC50) [uM]
d
KIN001-102 (AKTi) log10(IC50) [uM]
BRAF mut., skin
pancreas
RB1 mut., lung SCLC
lung SCLC
bone
leukemia, MAPK only down
Trametinib (MEKi) log10(IC50) [uM]
e
ZSTK474 (PI3K) log10(IC50) [uM]
lung SCLC, MAPK-PI3K down, TNFα down
BRAF mut., skin
lung SCLC
leukemia, lymphoma, MAPK only down
RDEA119-2 (MEKi) log10(IC50) [uM]

Supplementary Fig. S2 Distribution of subpopulations with differential drug response after segmentation when comparing multiple drugs. (A) Segmentation of pharmacological pattern of response for MAPK and AKT/PI3K pathway targets. There are five different MEK inhibitors (RDEA119-2, CI-1040, PD-0325901, selumetinib, and trametinib) showing the segmentation of 745 cell lines into subpopulations having distinct pharmacological patterns of response (see boxplots). Significance testing reveals enriched mutations in the subpopulations (blue boxes). **(B)** Scatter plot showing subpopulations (pink) sensitive to both trametinib (MEK inhibitor) and AS605240 (PI3K inhibitor). **(C)** Scatter plot showing subpopulations (yellow) sensitive to SB590885 (BRAF inhibitor) but resistant to GSK2126458 (PI3K inhibitor)**. (D)** Scatter plot showing subpopulations (green) sensitive to KIN001-102 (AKT inhibitor) but resistant to trametinib (MEK inhibitor). **(E)** Scatter plot showing subpopulations (blue) sensitive to RDEA119-2 (MEK inhibitor) but resistant to ZSTK474 (PI3K inhibitor) and sensitive to ZSTK474 but resistant to RDEA119-2. Enriched mutations, cancer tissue types, and/or expression pathway markers are labeled beside each subpopulation. Enriched expression pathway markers represent either the activated or inactive pathways in the subpopulation. They are labeled as "*pathway name*" up for activated pathways or down for inactive pathways.

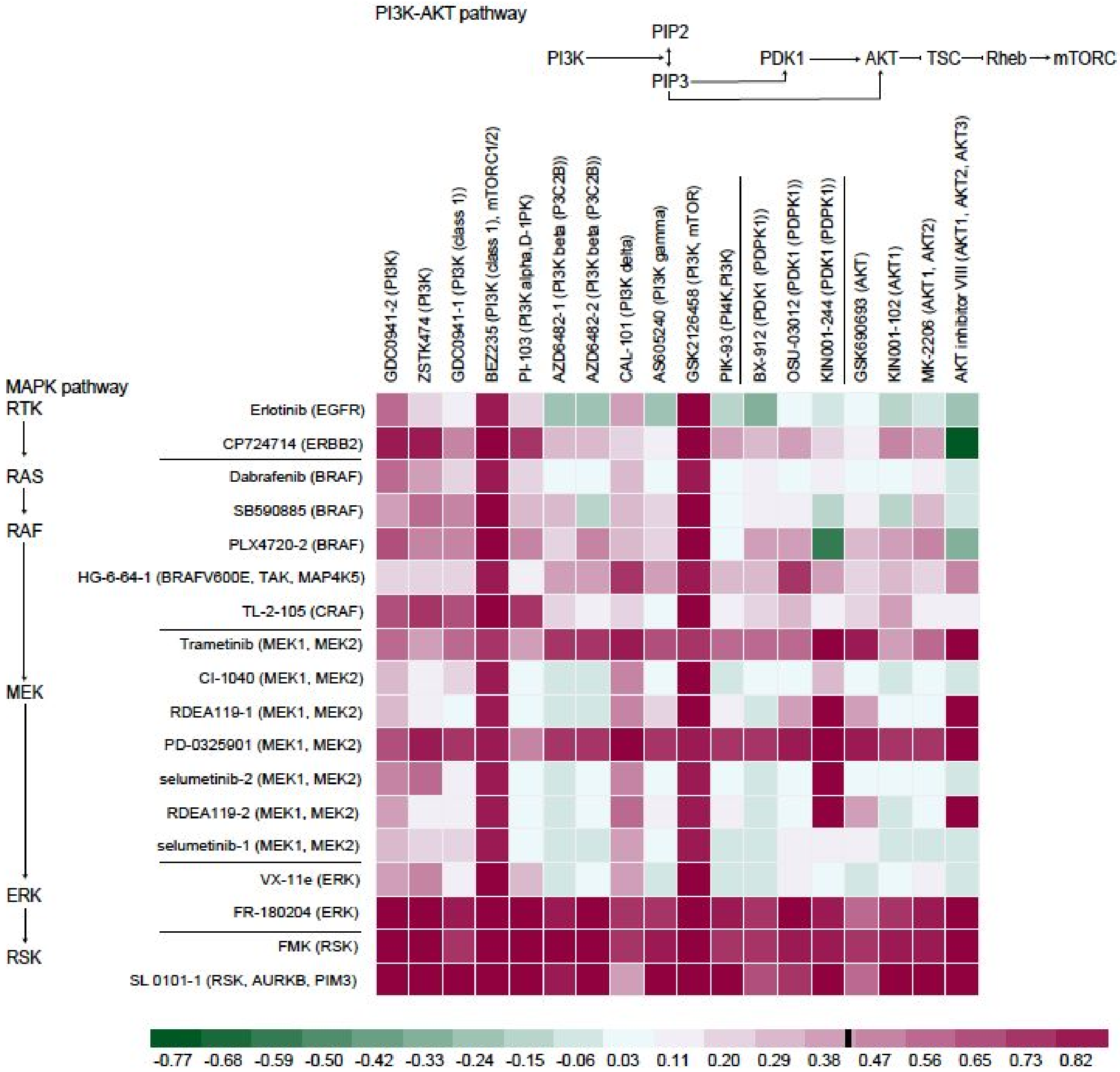

Supplementary Fig. S3 Average Pearson correlation coefficient of each drug pair. The average correlation coefficient of each drug pair was calculated by first constructing the variables vector as *x.* The average IC_{50} value of the subpopulations is represented as vector *c* and the size of the subpopulations as vector *s*. We compute $z = c \circ s$ and then *c* is stacked with *z* in sequence horizontally to construct the variables vector *x*. *z* is a vector where each entry is the summation of the IC_{50} value of each cell line grouped in the same subpopulation; the correlation coefficient matrix could be calculated by employing vector *x*. The average value in the correlation coefficient matrix is next calculated by taking the upper triangular matrix (represented as *U*) of the correlation coefficient matrix, then use a diagonal matrix which is 1 on the main diagonal to be subtracted from *U* to get the matrix *V*. Finally, the value of *V* is summed and divided by the number of unique subpopulation *l.* $l = n * (n-1)/2$ *n* is the number of the subpopulation resulting in the average correlation coefficient value for the drug pair.

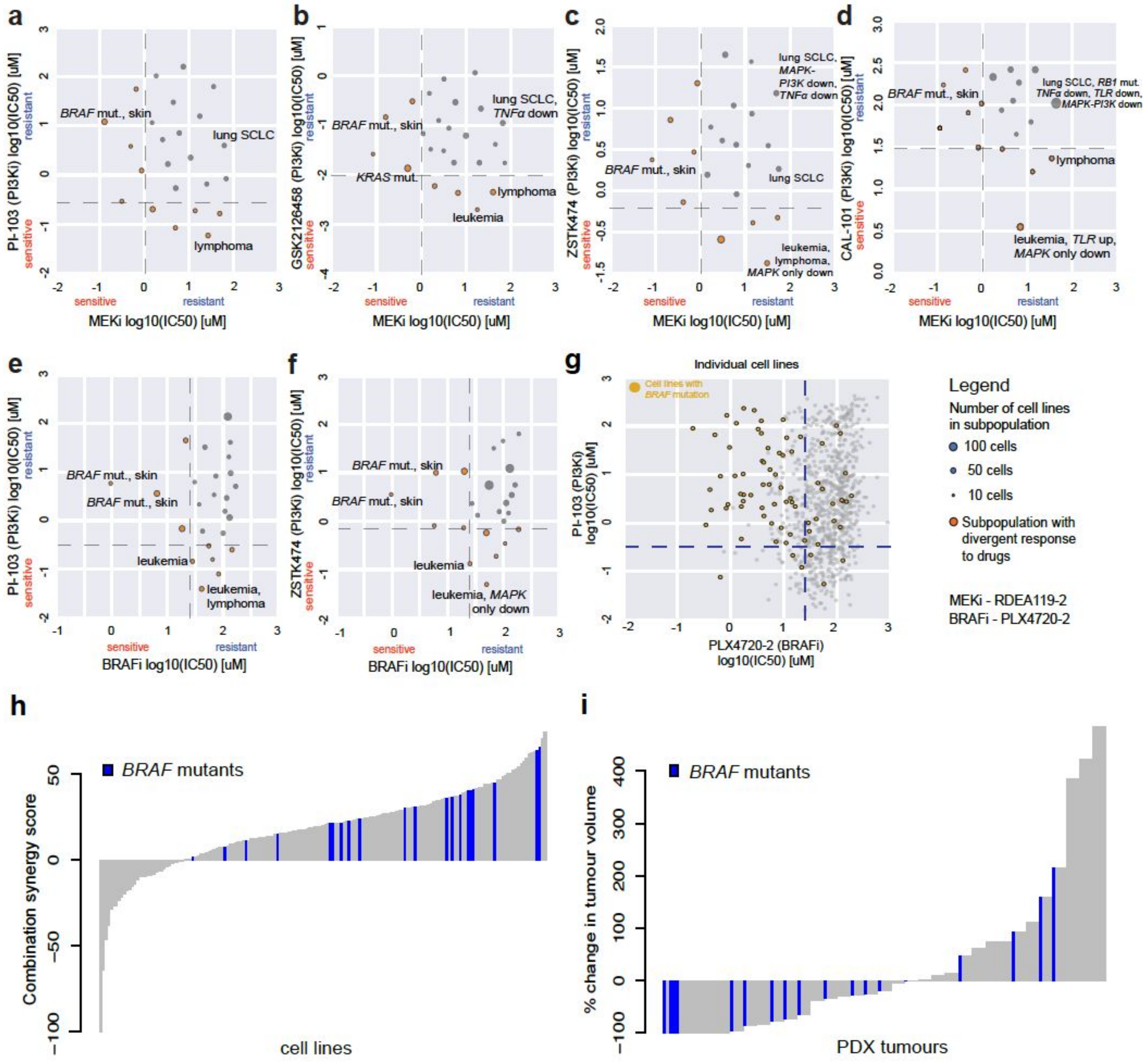

Supplementary Fig. S4 Efficacy identified in drug combinations showing divergent response. (A), (B), (C), (D) Subpopulations from comparison of response to MEK inhibitor (horizontal axis) to four different PI3K inhibitors (vertical axis) plotted by the average log(IC_{50}) of each subpopulation. **(E), (F)** Subpopulations resulting from comparison of BRAF inhibitor (horizontal axis) to two PI3K inhibitors (vertical axis). Enriched mutations, cancer tissue types, and/or expression pathway markers are labeled beside each subpopulation. Enriched expression pathway markers represent either the activated or inactive pathways in the subpopulation. They are labeled as "*pathway name*" up for activated pathways or down for inactive pathways. **(G)** Scatter plot of individual cell lines without subpopulations shown in panel **(E)**. All cell lines with *BRAF* mutation are coloured gold. The dashed lines indicate the 20th percentile of log(IC_{50}) values for each drug. **(H)** Response to combinations of MEK and PI3K inhibitors tested in cell lines, and **(I)** BRAF and PI3K inhibitors tested in patient-derived xenograft (PDX) tumours. Higher synergy score in cell lines indicate greater response to the combination therapy, and lower % change in tumor volume indicate greater response in PDX tumours.

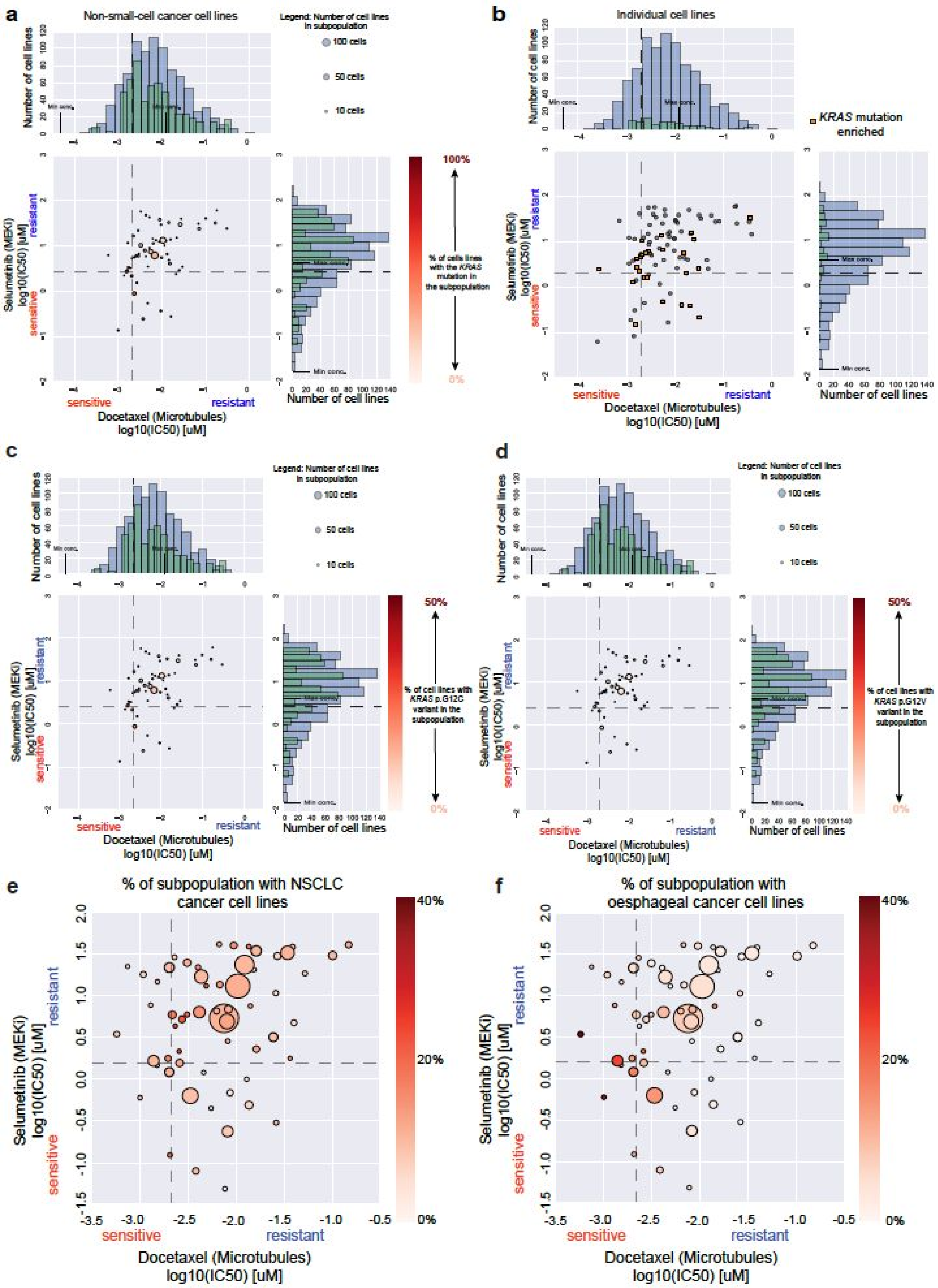

Supplementary Fig. S5 Analysis of the distribution of *KRAS* mutant NSCLC cell lines treated with docetaxel (microtubules) and selumetinib (MEK inhibitor). (A) Scatter plot showing the percentage of *KRAS* mutant NSCLC cell lines within each subpopulation. The subpopulations contain cell lines in all levels of the segmentation process. **(B)** Scatter plot illustrating the distribution of individual NSCLC cell lines treated with docetaxel and selumetinib. These cell lines are from subpopulations at the terminal level of the segmentation process. **(C)** Scatter plot showing the percentage of NSCLC cell lines with the *KRAS* p.G12C cell lines within each subpopulation. **(D)** Scatter plot showing the percentage of NSCLC cell lines with the *KRAS* p.G12V mutation within each subpopulation. **(E)** Scatter plot of subpopulations illustrating the percentage of NSCLC cell lines in each subpopulation of pan-cancer cell lines. **(F)** Same as panel **(E)** but for aerodigestive cancer cell lines.

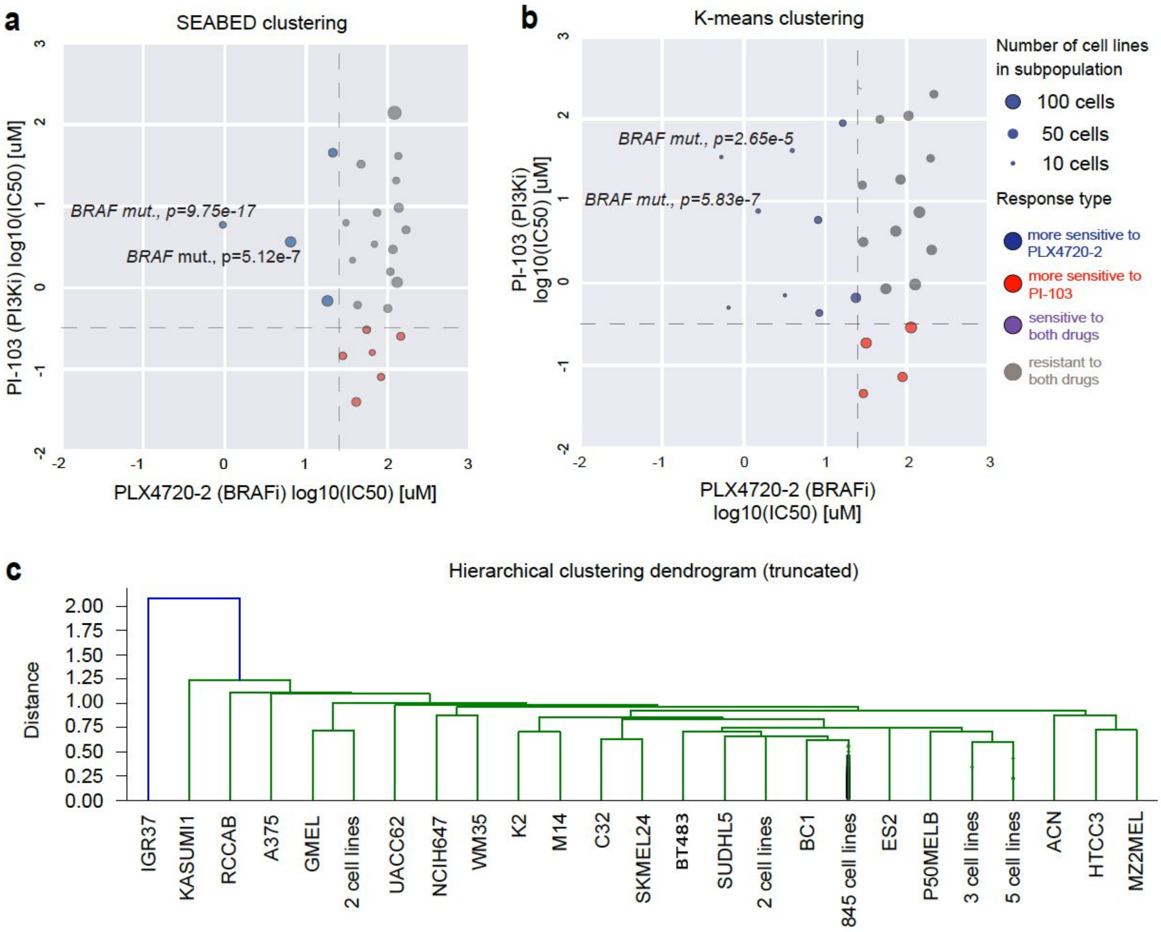

Supplementary Fig. S6 Comparison of clustering approaches for a drug pair. (A) Subpopulations and biomarkers produced by SEABED for the same drug pair (PLX4720-2 and PI-103). **(B)** Subpopulations identified using K-Means clustering for the same drug pair and biomarkers detected using the same technique. **(C)** Subpopulations identified using hierarchical clustering for the same drug pair. 20 of the clusters produced by hierarchical clustering contained only one cell line. Both K-Means and hierarchical clustering were set to generate the same number of clusters as SEABED.

Supplementary Tables

	Selumetinib + Docetaxel	Placebo + Docetaxel	Hazard Ratio	P-value
Participants (*KRAS* mutation positive) Analyzed	254	256		
Median Progression-Free Survival (Inter-Quartile Range)	3.9 (1.5 to 5.9)	2.8 (1.4 to 5.5)	0.93	0.4355
Median Overall Survival (Inter-Quartile Range)	8.7 (3.6 to 16.8)	7.9 (3.8 to 20.1)	1.05	0.6431

Supplementary Table S1 Primary and secondary endpoints for the SELECT-1 Trial evaluating the efficacy of selumetinib and docetaxel in locally advanced or metastatic NSCLC (Jänne et al., 2017).

	K-Means	Hierarchical Clustering	SEABED
Minimum	4	1	20
Median	36	1	33
Maximum	81	846	83

Supplementary Table S2 Minimum, median and maximum of subpopulation sizes for different segmentation techniques for PLX4720-2 (BRAF inhibitor) and PI-103 (PI3K inhibitor) in Fig. 3.

	K-Means	Hierarchical Clustering	SEABED
Silhouette Coefficient	0.323 ± 0.037	0.036 ± 0.018	0.231 ± 0.056
RMSSTD	0.228 ± 0.135	0.854 ± 0.050	0.198 ± 0.103

Supplementary Table S3 Mean pairwise cluster validation results for two different segmentation techniques for PLX4720-2 (BRAF inhibitor) and PI-103 (PI3K inhibitor) in Fig. 3. Larger silhouette values indicate greater separation, while smaller values of RMSSTD indicate higher cluster homogeneity.

Key Resources Table

REAGENT or RESOURCE	SOURCE	LOCATION

Deposited Data		
The Genomics of Drug Sensitivity in Cancer (GDSC) database	(Garnett et al., 2012; Iorio et al., 2016)	https://www.cancerrxgene.org/
Cancer Cell Line Encyclopedia (CCLE)	(Barretina et al., 2012)	https://portals.broadinstitute.org/ccle
Cancer Therapeutics Response Portal (CTRP)	(Basu et al., 2013; Rees et al., 2016; Seashore-Ludlow et al., 2015)	https://portals.broadinstitute.org/ctrp/
Menden et al. dataset	(Menden et al.)	
Gao et al. dataset	(Gao et al., 2015)	
Raw and analysed datasets	This paper	Supplementary Tables S4 and S5
Software and Algorithms		
SEABED code	https://github.com/szen95/SEABED	N/A
Matplotlib	(Hunter, 2007)	N/A
Numpy	(Oliphant, 2006)	N/A
Pandas	(McKinney, 2017)	N/A
Bioconductor (R)	www.bioconductor.org	N/A
graph-tool	https://graph-tool.skewed.de	N/A

References

Jänne, P.A., van den Heuvel, M.M., Barlesi, F., Cobo, M., Mazieres, J., Crinò, L., Orlov, S., Blackhall, F., Wolf, J., Garrido, P., et al. (2017). Selumetinib Plus Docetaxel Compared With Docetaxel Alone and Progression-Free Survival in Patients With KRAS-Mutant Advanced Non–Small Cell Lung Cancer. JAMA *317*, 1844.

Barretina, J., Caponigro, G., Stransky, N., Venkatesan, K., Margolin, A.A., Kim, S., Wilson, C.J., Lehár, J., Kryukov, G.V., Sonkin, D., et al. (2012). The Cancer Cell Line Encyclopedia enables predictive modelling of anticancer drug sensitivity. Nature *483*, 603–607.

Basu, A., Bodycombe, N.E., Cheah, J.H., Price, E.V., Liu, K., Schaefer, G.I., Ebright, R.Y., Stewart, M.L., Ito, D., Wang, S., et al. (2013). An interactive resource to identify cancer genetic and lineage dependencies targeted by small molecules. Cell *154*, 1151–1161.

Gao, H., Korn, J.M., Ferretti, S., Monahan, J.E., Wang, Y., Singh, M., Zhang, C., Schnell, C., Yang, G., Zhang, Y., et al. (2015). High-throughput screening using patient-derived tumor xenografts to predict clinical trial drug response. Nat. Med. *21*, 1318–1325.

Garnett, M.J., Edelman, E.J., Heidorn, S.J., Greenman, C.D., Dastur, A., Lau, K.W., Greninger, P., Thompson, I.R., Luo, X., Soares, J., et al. (2012). Systematic identification of genomic markers of drug sensitivity in cancer cells. Nature *483*, 570–575.

Hunter, J.D. (2007). Matplotlib: A 2D Graphics Environment. Computing in Science & Engineering *9*, 90–95.

Iorio, F., Knijnenburg, T.A., Vis, D.J., Bignell, G.R., Menden, M.P., Schubert, M., Aben, N., Gonçalves, E., Barthorpe, S., Lightfoot, H., et al. (2016). A Landscape of Pharmacogenomic Interactions in Cancer. Cell *166*, 740–754.

McKinney, W. (2017). Python for Data Analysis: Data Wrangling with Pandas, NumPy, and IPython ("O'Reilly Media, Inc.").

Menden, M.P., Wang, D., Guan, Y., Mason, M., Szalai, B., Bulusu, K.C., Yu, T., Kang, J., Jeon, M., Wolfinger, R., et al. A cancer pharmacogenomic screen powering crowd-sourced advancement of drug combination prediction.

Oliphant, T.E. (2006). A Guide to NumPy.

Rees, M.G., Seashore-Ludlow, B., Cheah, J.H., Adams, D.J., Price, E.V., Gill, S., Javaid, S., Coletti, M.E., Jones, V.L., Bodycombe, N.E., et al. (2016). Correlating chemical sensitivity and basal gene expression reveals mechanism of action. Nat. Chem. Biol. *12*, 109–116.

Seashore-Ludlow, B., Rees, M.G., Cheah, J.H., Cokol, M., Price, E.V., Coletti, M.E., Jones, V., Bodycombe, N.E., Soule, C.K., Gould, J., et al. (2015). Harnessing Connectivity in a Large-Scale Small-Molecule Sensitivity Dataset. Cancer Discovery *5*, 1210–1223.